Quantum transport of Dirac fermions in graphene nanostructures

Philippe Dollfus[1], Viet-Hung Nguyen[1,2], Van-Nam Do[3] and Arnaud Bournel[1]
[1] Institute of Fundamental Electronics (IEF), Univ. Paris-Sud, CNRS, UMR 8622, Orsay, France
[2] Institute of Physics, Vietnamese Academy of Science and Technology, Hanoi, Vietnam
[3] Hanoi Advanced School of Science and Technology, Hanoi Univ. of Technology, Hanoi, Vietnam
e-mail: philippe.dollfus@u-psud.fr

***Abstract*— An effective approach of quantum transport of Dirac carriers in mono- and bi-layer graphene structures and devices is presented. Initially based on the Green's function formalism to treat the Dirac Hamiltonian of massless particles in two-dimensional mono-layer graphene, the model has been extended to to small bandgap materials and to bi-layer graphene with massive carriers. It is applied to investigate some transport problems as the minimum conductivity, the tunneling properties the spin-polarized transport through single-barrier structures, and the operation of graphene field-effect transistors.**

Keywords - graphene; Green's function, Dirac fermions

I. INTRODUCTION

Though it is unsuitable for standard digital applications, the gapless character of graphene with chiral massless Dirac carriers gives to this material unusual and attractive transport properties which deserve to be considered carefully [1]. Some of the most remarkable transport properties are the finite minimum conductivity [2], the unconventional quantum Hall effect [3,4], and the Klein paradox [5]. Very high room-temperature mobilities exceeding 15 000 cm^2/Vs have been measured and values of 200 000 cm^2/Vs have been shown to be achievable [6,7] with proper choice of substrate or by suspended graphene. Additionally, there are several ways of inducing bandgap in graphene, which still enlarge the possible fields of application. The first idea is to cut mono-layer graphene into nanoribbons to benefit from induced quantum confinement effect. Alternatively, the interaction with an SiC substrate can break the symmetry of the two sub-lattices forming the graphene crystal, which can open a bandgap of up to 0.26 eV [8]. A similar bandgap may be also induced in bi-layer graphene by applying a vertical electric field [9,10].

While most of graphene device simulations are based on the non-equilibrium Green's function (NEGF) formalism to treat an atomistic tight-binding Hamiltonian for small semiconducting nanoribbons (GNRs) [11-14], we use here an effective model for wide 2D graphene samples based on the Dirac Hamiltonian for relativistic-like massless carriers [15]. This model may be even extended to small bandgap materials and to bi-layer graphene [16]. Though not suitable for nanoribbons, it makes possible to study a wide variety of devices and transport problems on 2D graphene samples. In addition to the description of the model, we present here its application to some transport problems in mono-layer or bi-layer graphene, such as the influence of impurity/vacancy on the conductivity, the specific tunneling properties of carriers through single barriers, the spin-polarized transport in graphene structures, and the simulation of graphene FETs.

II. MODEL

To describe the electronic structure of the honeycomb arrangement of carbon atoms in a graphene sheet, a simple nearest-neighbor tight-binding description can be conveniently used, with $a_c = 0.142$ nm as carbon-carbon distance and $t = 2.7$ eV as integral overlap between p_z orbitals. It leads to a unique band structure with two bands which touch at six points, the so-called Dirac or neutrality points, which means that graphene has zero bandgap. For symmetry reasons, these points are reduced to a pair of independent points, noted K and K'. The bands have a conical shape (Fig. 1) well described at first order by the linear dispersion

$$E(\mathrm{k}) = \pm\hbar v_F \sqrt{k_x^2 + k_y^2} \qquad (1)$$

where $v_F = 3a_c t/2\hbar \approx 10^6$ m/s is the Fermi velocity and $\mathbf{k} = (k_x, k_y)$ is the 2D-wavevector of the particle. Carriers in graphene are thus massless. Moreover, the fact that the structure of graphene contains two sublattices, noted A and B, gives to the particle Hamiltonian the form of a relativistic Dirac Hamiltonian

$$H = \hbar v_F \left(k_x \sigma_x + k_y \sigma_y\right) + U(x)\sigma_0 \qquad (2)$$

where $\sigma_{x,y,z}$ are the Pauli matrices, σ_0 is the identity matrix and U stands for the external potential energy. In condensed matter, electrons and holes are usually described by separate Schrödinger equations. In contrast, electron and hole states in graphene are interconnected and have properties analogous to the charge conjugation symmetry in quantum electrodynamics. It is a consequence of the graphene's crystal symmetry, i.e., the equivalence of two carbon sublattices A and B. Therefore, graphene's quasi-particles are described by two component wave-functions, very similar to the spinor wave-functions in quantum electrodynamics, but the "spin" index for graphene specifies the sublattice rather than the real spin of electrons and is called pseudospin σ. To include in the Hamiltonian (2) the bandgap opening possibly due to substrate

This work was partially supported by the European Community through the Network of Excellence NANOSIL (ICT-216171) and by the French ANR through the project NANOSIM_GRAPHENE (ANR-09-NANO-016). The work at Hanoi supported by the Vietnamese National Foundation for Science and Technology Development (NAFOSTED) under Project No. 103.02.64.09.

978-1-4244-9382-1/10/$26.00 ©2010 IEEE

influence, we just have to add the mass term $m v_F^2 \sigma_z$ corresponding to the bandgap $E_G = 2 m v_F^2$.

The tight binding model can be easily extended to bi-layer graphene (Fig. 2) by considering the hopping energy between atoms A_1 and A_2 of the two layers. After first order expansion close to the K-points, the energy dispersion writes

$$E^2(\mathbf{k}) = \hbar^2 v_F^2 k^2 + \frac{\gamma^2}{2} + \frac{\Delta^2}{4} \pm \sqrt{\left(\gamma^2 + \Delta^2\right)\hbar^2 v_F^2 k^2 + \frac{\gamma^4}{4}} \quad (3)$$

where Δ stands for the difference of potential between the graphene layers. Now carriers have a finite effective mass. If $\Delta = 0$ and $\hbar v_F k << \gamma$, the energy dispersion may simplify in

$$E(\mathbf{k}) = \pm \hbar^2 k^2 / 2m \quad (4)$$

with the effective mass $m = \gamma / 2 v_F^2 \approx 0.045 m_0$. For finite values of Δ a bandgap between conduction and valence band opens as

$$E_G = \gamma \Delta / \sqrt{\Delta^2 + \gamma^2} \quad (5)$$

In case of strong asymmetry $\Delta >> \gamma$, the bandgap reaches the limit value $E_G \approx \gamma$ and for weak asymmetry, we have $E_G \approx \Delta$, which suggests that a bandgap may be simply obtained by applying an electric field between the layers [9,10].

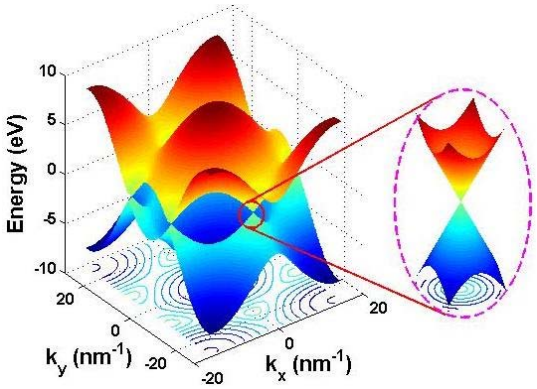

Figure 1. Full energy dispersion of the graphene honeycomb lattice and zoom in showing a low-energy Dirac cone close to a Dirac point.

For bi-layer graphene the Hamiltonian (2) writes

$$H = \begin{bmatrix} \hbar v_F \boldsymbol{\sigma} \cdot \mathbf{k} + U_1 & \tau \\ \tau^\dagger & \hbar v_F \boldsymbol{\sigma} \cdot \mathbf{k} + U_2 \end{bmatrix} \text{ with } \tau = \begin{bmatrix} 0 & 0 \\ \gamma & 0 \end{bmatrix} \quad (6)$$

where the sub-matrix τ describes the coupling between the layers and $\Delta = U_2 - U_1$.

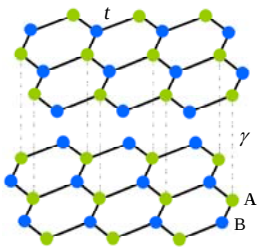

Figure 2. Lattice structure of bilayer graphen with hopping energies τ and γ between nearest neighbor atoms of the same and of different layers

An efficient calculation method based on the NEGF formalism has been developed to solve the Dirac equation by rewriting the Hamiltonians (2) or (6) within a tight-binding formulation in a new basis $\{|x_n\rangle, |k_y\rangle\}$ using the arbitrary mesh spacing $a = x_n - x_{n-1} = 0.2$ nm [15-17]. The device Green's function is defined as

$$G(E) = \left[E + i\eta - H - \Sigma_L - \Sigma_R - \Sigma_S\right]^{-1} \quad (7)$$

where Σ_L and Σ_R are the self-energy coupling the device to left and right contacts, respectively, and Σ_S stands for the self-energy describing any possible scattering mechanism. The local density of states and the transmission coefficient are defined as

$$\rho(x_n, E) = -\frac{1}{\pi} \mathrm{Im}\left[G_{n,n}(E)\right] \text{ and } T(E) = Tr\left[\Gamma_L G \Gamma_R G^\dagger\right] \quad (8)$$

where the tunneling rate at the left (right) contact is defined as $\Gamma_{L(R)} = i\left(\Sigma_{L(R)} - \Sigma_{L(R)}^\dagger\right)$. The current density is given by

$$J = \frac{2e}{\pi h} \int_{-\infty}^{+\infty} dE\, dk_y\, T(E, k_y) \left[f_L(E) - f_R(E) \right] \quad (9)$$

where $f_{L(R)}$ is the Fermi function in the left (right) contact. Finally, for device of length L_x the conductivity is defined in the low-temperature limit as

$$\sigma(E_F) = \frac{4e^2}{\pi h} \frac{L_x}{3a_c} \frac{1}{t} \int dE_y\, T(E_F, E_y) \quad (10)$$

where the transverse energy is defined as $E_y = \hbar v_F k_y$.

III. MINIMUM CONDUCTIVITY IN MONO-LAYER GRAPHENE

Because of linear energy-dependence of the density of states $\rho(E) = |E| / \pi (\hbar v_F)^2$, graphene was not expected to conduct electrical current in the neutral state. However, many experiments have demonstrated unambiguously the existence of a finite value of conductivity σ_{min} at the Dirac neutrality

points (DNPs) [2,17]. In spite of significant spreading from sample to sample, experimental data of σ_{min} converge to an order of magnitude of e^2/h [17]. From the theoretical point of view the finite value $\sigma_{min} = 4e^2/\pi h$, i.e. π times smaller than the value initially reported in the early stages of graphene research [2]. Great efforts have been made to explain this apparent mystery missing of π and the spreading of experimental data, possibly due to the effect of disorder and charged impurities (see [18] for a review of this problem).

Recently, our Green's function approach allowed us to show some effects of metallic electrodes and impurities on the transport properties of graphene sheets deposited onto a substrate. Indeed, previous investigations of the effect of contacts have suggested that the metallic electrode-graphene contact are in practice in the limit of strong coupling which governs the asymmetric V-shape curve of the conductivity versus the charge carrier density with a single minimum value of the order of e^2/h [19]. Importantly, it has been also shown that contact-induced states may deeply penetrate into the graphene active region between the electrodes and thus enhance the density of states (DOS) at the charge neutrality point (NP). Consequently the conductivity minimum occurring at NP can rise up to the range of experimental data, i.e., $4e^2/\pi h$-$12\ e^2/\pi h$ [20]. In practice, graphene samples however usually have a long active region, in the micrometer scale, and the penetration effect of contacted-induced states therefore may be expected to be negligible. In this case, the role of impurities adsorbed onto the graphene surface appears to be dominant. Let us consider a typical short-range impurity scattering potential in the form $V(\mathbf{r}-\mathbf{R}_i) = U \cdot \delta(\mathbf{r}-\mathbf{R}_i)$. It should be noted that to include properly the DOS enhancement effect at NP, the self-consistent T-matrix calculation scheme should be used to account for the effect of multiple scattering on a single impurity. In this approximation the self-energy associated with the considered scattering process under is given by

$$\Sigma_{imp} = N U \left\{ 1 + \frac{U(E-\Sigma_{imp})}{2\pi(\hbar v_F)^2} \ln\left[1 - \left(\frac{E_c}{E-\Sigma_{imp}} \right)^2 \right] \right\}^{-1} \qquad (11)$$

where N is the impurity density and E_c is an energy cutoff. As expected, this equation results in the self-energy with a peak of the imaginary part at the Dirac point $E = 0$ [20]. As a consequence the density of states is enhanced to finite values around this point.

The conductivity calculated for 100 nm-long structures in the limit of large U is plotted in Fig. 3 for several values of the impurity density. In the range 0-3×10^{10} cm^{-2}, we observe a continuous increase of σ_{min} from one to five times of $4e^2/\pi h$. However, it does not mean that raising further the impurity density will monotonically increase the value of σ_{min} since not only the imaginary part but also the real part of the self-energy increase. Consequently, at higher density the electrostatic potential can change dramatically and thus localize electronic states. To illustrate this point we additionally show in Fig. 3 the red dashed curve of the conductivity extracted for $N = 10^{11}$ cm^{-2}, which exhibits a minimum point lower than that of $4e^2/\pi h$. This detailed analysis of impurity scattering using appropriate self-energy is very consistent with experimental investigations and explain the large spreading in measured conductivity data.

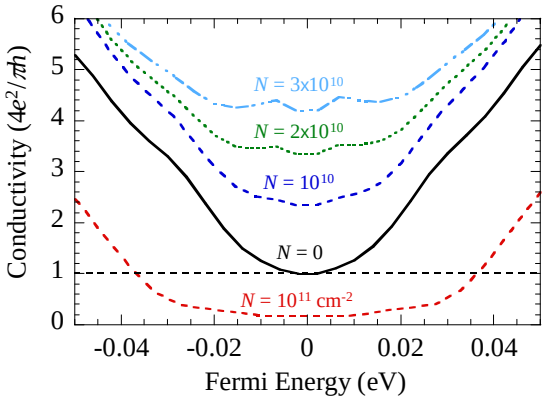

Figure 3. Conductivity in 100 nm-long graphene structures for different values of impurity density.

IV. TRANSPORT IN SINGLE-BARRIER GRAPHENE STRUCTURES

We now apply the Green's function approach of Dirac's equation to the investigation of charge transport properties in a rectangular single-barrier graphene structure. Though simple, this structure may highlight some fundamental microscopic features of charges in graphene, e.g., the charge-conjugation symmetry, the chirality of particles and the Klein tunnelling. An electron with energy E propagating in the positive direction originates from the same branch of the electronic spectrum as the hole of energy -E propagating in the opposite direction. This yields the important consequence that electrons and holes of the same branch have the pseudospin σ in the same direction, which is parallel to the momentum for electrons and antiparallel for holes. This feature may be seen as the chirality character of quasi-particles in graphene.

In Fig. 4 we display the local density of states and the transmission coefficient T for a structure of barrier width W and height U_0 of 20 nm and 0.55 eV, respectively, for a transverse energy $E_y = 50$ meV and a bias voltage $V_b = 0.3$ V, to highlight the chiral property of transport. At finite values of E_y the transmission coefficient exhibits an energy valley of width $2E_y$, centered on the U_0 value. This valley separates the transmission coefficient into three parts, called here T_N and T_K, corresponding to the energy ranges $[U_0 + |E_y| - eV_b/2, +\infty]$ above the barrier and $[|E_y|, U_0 - |E_y| - eV_b/2]$ through the barrier, respectively. In contrast to the case of ordinary semiconductors, the transmission does not exponentially decay through the barrier but exhibits oscillations with resonant-like subpeaks reaching the value of 1. The appearance of such peaks is essentially due to the resonance or the good matching of electron states and hole states outside/inside the barrier region, respectively. The corresponding tunneling regime is called chiral or Klein tunneling. An additional tunneling regime appears at negative energy, separated from the chiral tunneling by a gap of width $2E_y$. It is the band-to-band tunneling from the valence to the conduction band.

For $E_y = 0$ the transmission coefficient is equal to 1 (not shown), which is nothing, but the manifestation of the so-called Klein's paradox, which states that the potential barrier is transparent for zero-angle incident relativistic particles whatever the barrier height and width. It has been shown that chiral tunneling may give rise to a negative differential conductance in such a single barrier structure but this effect is actually severely limited by the occurring of band-to-band tunneling when increasing the bias voltage, as a consequence of zero bandgap [15].

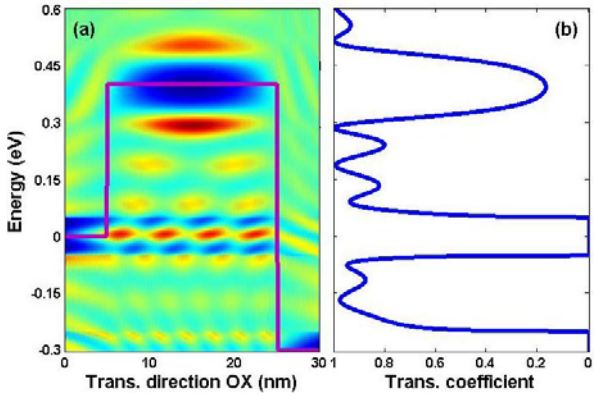

Figure 4. LDOS and transmission coefficient in the single barrier mono-layer graphene structure with finite bias $V_b = 0.3$ eV. Other parameters are $E_y = 50$ meV, $U_0 = 0.55$ eV, and $L = 20$ nm.

Monolayer structure, bilayer graphene share some similaruties but also have some differences. For instance, charge carriers in bilayer graphene have a parabolic gapless energy dispersion around the K points, which means they are massive quasi-particles with a finite density of states at zero energy, as in conventional materials. The origin of this unusual energy dispersion is in the lattice structure of bilayer graphene with four equivalent sublattices. However, these quasi-particles are still chiral and described by spinor wave-functions, similar to relativistic quasi-particles in monolayer graphene.

Another striking difference appears in the transmission through a single barrier. While normal incident particles are all transmitted through a mono-layer barrier, they are all reflected by a bi-layer graphene barrier. For a finite $E_y = 50$ meV, the chiral transmission coefficient exhibits much higher and thinner resonant peaks than in the mono-layer case, as illustrated in the LDOS and transmission plotted in Fig. 5.

These peaks originate some interesting features in the *I-V* characteristics, as in Fig. 6 where we plot the zero-temperature current density as a function of bias voltage for different barrier height and a barrier length of 20 nm. Some of the curves exhibit an NDC behavior, more pronounced than in the mono-layer case, though still limited to a peak-to-valley ratio of about 1.8. However, the most interesting feature is in the periodic oscillations of the current when tuning the barrier height, as a consequence of the sweeping of thin hole bound states in the barrier. It results in strong oscillations of the transconductance (Fig. 7) between negative and positive values, with phase shift depending bias voltage. It is worth noting that in psite of smearing effect, the oscillations of transconductance are persistent at finite temperature T = 77 K (blue circles) end even at room temperature (not shown).

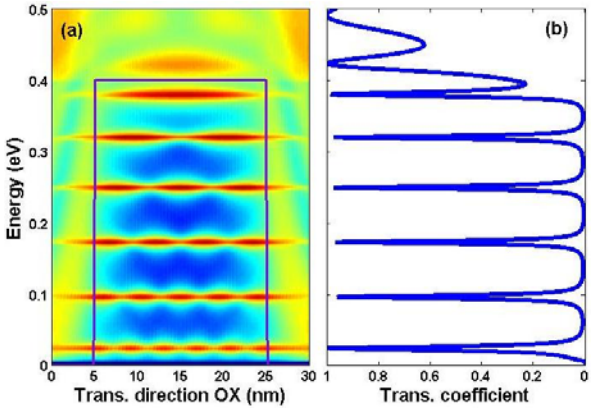

Figure 5. LDOS and transmission coefficient in a single barrier bi-layer graphene structure under zero bias. Other parameters are $E_y = 50$ meV, $U_0 = 0.4$ eV, and $L = 20$ nm.

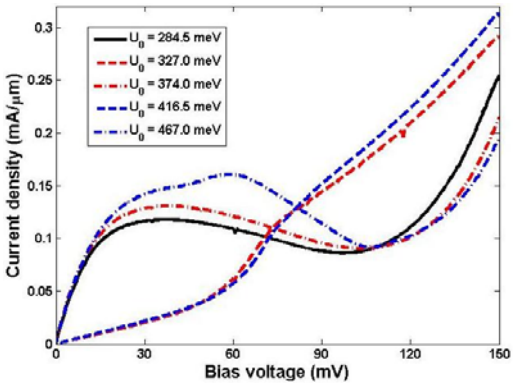

Figure 6. Low temperature current as a function of bias voltage in a single barrier bi-layer graphene structure of barrier length $L = 20$ nm for different barrier heights.

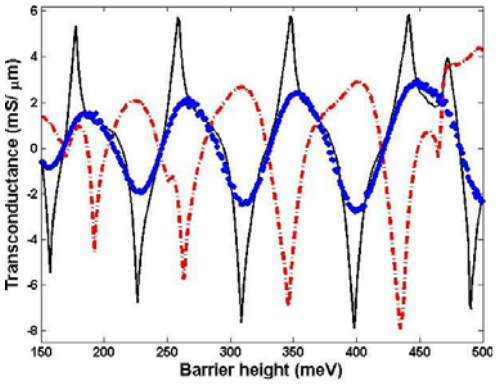

Figure 7. Transconductance as a function of barrier height at zero temperature for $V_b = 40$ meV (black solid line) and $V_b = 105$ meV (dashed-dotted line) for the same structure as in Fig. 6. Blue circles correspond to results at $T = 77$ K ($V_b = 40$ meV).

We now consider the effect of bandgap opening induced by a vertical electric field applied normal to the double-gate bi-layer structure. For a difference of potential $\Delta = U_2 - U_1$ between the two layers, a bandgap given by (5) appears at the top of the barrier, as illustrated in the local DOS and transmission coefficient displayed in Fig. 8. Below the bandgap, some hole bound states are still present, though the corresponding transmission peaks do not reach the value of 1.

Though limited to a few hundreds of meV this bandgap is expected to offer the possibility of switching off the current, at least patially. It is illustrated in Fig. 9 where we plot the current at different temperatures as a function of Δ for $V_b = 50$ mV and $U_m = (U_2 + U_1)/2 = 75$ meV $= E$. The current reaches its maximum value for $\Delta = 0$ and rapidly decreases when the gap increases. Of course the slope of the curve reduces when increasing the temperature but persists at room temperature. Similar results have been obtained experimentally [21].

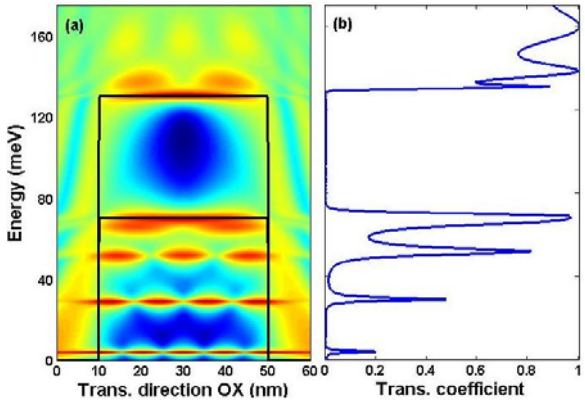

Figure 8. Field-effect bandgap opening in the LDOS and the transmission coefficient of a single barrier double-gate bi-layer graphene structure under zero bias (L = 40 nm, E_y = 50 meV, U_0 = 0.4 eV)

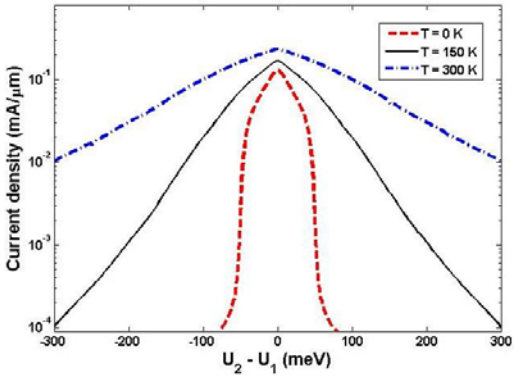

Figure 9. Current as a function of potential difference Δ fot three temperatures a single barrier double-gate bi-layer graphene structure. Other parameters: $U_m = 75$ meV $= E_F$, L = 40 nm, $V_b = 50$ meV.

V. SPIN-POLARIZED TRANSPORT IN GRAPHENE STRUCTURES

Thanks to very weak spin-orbit interaction leading to spin flip length higher than 1.5 μm [22], graphene also offer a high potential for spintronics. Recent works have shown or suggested that magnetism can be introduced in graphene by doping or defect, by applying an external field, or by proximity effect of a ferromagnetic insulator [23]. It led us to consider the possibility of controlling the spin-polarized current in graphene sheets using a ferromagnetic gate. For such a study the model has been slightly modified by adding a Zeeman term $-\sigma h$ where h is the exchange splitting energy and σ describes the up/down spin states. It means that the barrier height is spin-dependent.

For a monolayer graphene structure with a single ferromagnetic barrier, we see in Fig. 10 the oscillation behavior of the conductance of each spin channel and of the spin polarization $P = (G_\uparrow - G_\downarrow)/(G_\uparrow + G_\downarrow)$ as a function of barrier height for h = 25 meV. The spin polarization reaches the maximum value of about 20% in monolayer graphene. This oscillation behavior obviously comes from the resonant tunneling of electron states through the hole bound states in the barrier.

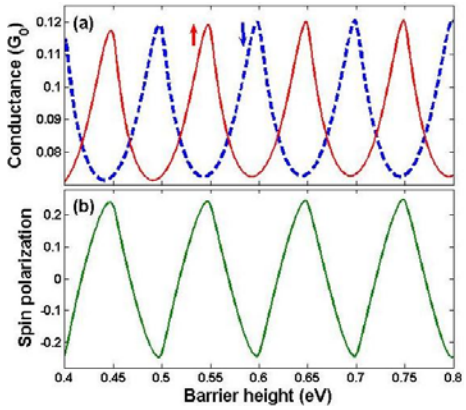

Figure 10. (a) Spin up and spin down conductance and (b) spin polarization in a single ferromagnetic gate monolayer graphene structure as a function of the gate barrier height, for L = 20 nm, E_F = 100 meV and h = 25 meV.

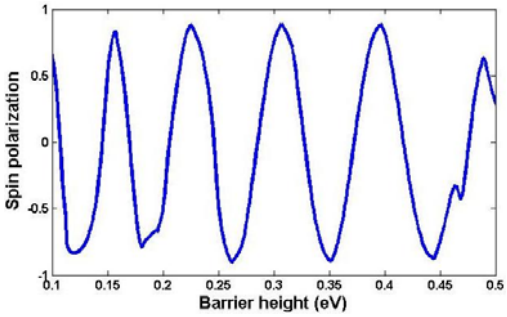

Figure 11. Spin polarization in a single ferromagnetic gate bilayer graphene structure as a function of the gate barrier height, for L = 20 nm, E_F = 75 meV and h = 22.5 meV.

Thanks to thinner resonant peaks in the chiral tunneling transmission, higher spin polarization may even be reached in bilayer structures, as shown in Fig. 11 with a nearly ideal value of 95%. Though experimental confirmation is still needed, such predictions open the way for spintronics application with high gate-controlled tunability of spin polarization.

VI. GRAPHENE FIELD-EFFECT TRANSISTORS

Now we consider the simulation of monolayer graphene based field-effect transistors (GFETs). In this purpose the transport model is here coupled with a 2D Poisson solver, as in Section III, to provide self-consistent results. The simulated transistor has a gate length L_G = 15 nm and source/drain extensions $L_S = L_D$ = 20 nm [24]. We consider both cases of gapless and finite bandgap possibly induced by interaction with SiC substrate [8].

In the case of massless electrons, the local DOS is shown in Fig. 12 with the self consistent potential for V_{GS} = -1 V and V_{DS} = 0.2V. We see again the hole bound states in the barrier

likely to give rise to Klein tunneling in the regime of low gate voltage. However, in such transistors, band-to-band tunneling is likely to play a more important role than Klein tunneling. In particular it degrades strongly the current saturation in gapless FET (Fig. 13a). Clearly, the bandgap opening improves significantly the device operation, as shown in Fig. 13. The bandgap-induced suppression of band-to-band tunneling improves the current saturation at large V_{DS} (Fig. 13a) and the on/off current ratio (Fig. 13b) which is known to very poor in gapless graphene transistors. It reaches about 100 for a bandgap E_G = 260 meV. Though it is probably not high enough for digital applications, it opens the road for efficient transistors likely to operate in the THz regime, as recently demonstrated experimentally.

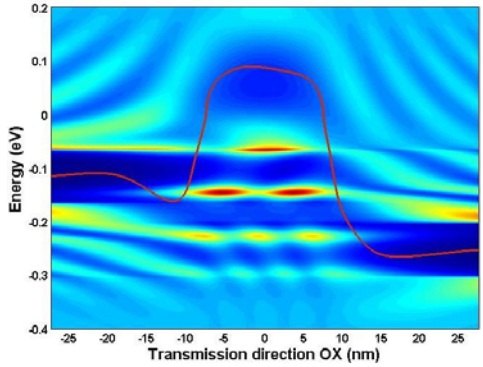

Figure 12. LDOS in the simulated transistor for E_y = 50 meV and self-consistent potential (V_{GS} = 1 V, V_{DS} = 0.2 V).

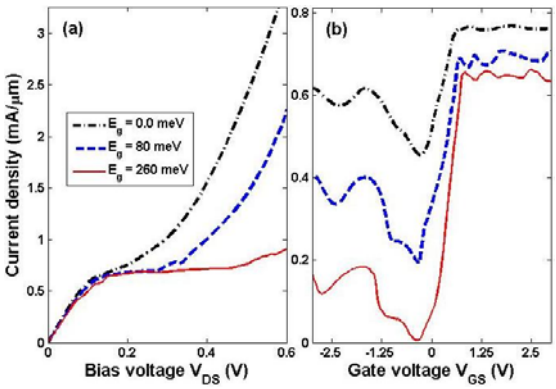

Figure 13. Current density at T = 77 K as a function (a) of drain voltage for V_{GS} = 1 V and (b) of gate voltage for V_{DS} = 0.2 V and for for different values of energy bandgap.

VII. Conclusion

We have presented a powerful simulator of Dirac fermions transport in graphene structures suitable for mono- and bi-layer graphene and for both types of massless and massive particles. It includes all features of chiral particles. It has been applied here to study several transport problems, including the minimum conductivity in graphene, spin-polarized transport and graphene-based transistors.

Acknowledgment

The authors would like to thank Van-Lien Nguyen for many useful discussions.

References

[1] A. K. Geim and K. S. Novoselov, "The rise of graphene", Nature Mater., vol. 6, pp. 183-191, 2007.

[2] K. S. Novoselov et al., "Two-dimensional gas of massless Dirac fermions in graphene", Nature, vol. 438, pp. 197-200, 2005.

[3] Y. Zhang, Y.W. Tan, H. L. Stormer, and P. Kim, "Experimental observation of the quantum Hall effect and Berry's phase in graphene",. Nature, vol. 438, pp. 201–204, 2005.

[4] K. S. Novoselovet al., "Unconventional quantum Hall effect and Berry's phase of 2π in bilayer graphene", Nature Phys., vol. 2, pp. 177–180, 2006.

[5] M. I. Katsnelson, et al., "Chiral tunnelling and the Klein paradox in graphene", Nature Phys., vol. 2, pp. 620-625, 2006.

[6] J.-H. Chen, C. Jang, S. Xiao, M. Ishigami, and M. S. Fuhrer, "Intrinsic and extrinsic performance limits of graphene devices on SiO2", Nature Nanotech., vol. 3, pp. 206-209, 2008.

[7] S.V. Morozov et al., "Giant Intrinsic Carrier Mobilities in Graphene and Its Bilayer", Phys. Rev. Lett., vol. 100, 016602, 2008.

[8] S. Y. Zhou et al., "Substrate-induced bandgap opening in epitaxial graphene", Nature Mater., vol. 6, pp. 770-775, 2007.

[9] E. V. Castro et al., "Biased bilayer graphene: semiconductor with a gap tunable by the electric field effect", Phys. Rev. Lett., vol. 99, 216802, 2007

[10] Y. Zhang et al., "Direct observation of a widely tunable bandgap in bilayer graphene", Nature, vol. 459, pp. 820-823, 2009.

[11] G. Fiori and G. Iannaccone, "Simulation of graphene nano-ribbon field-effect transistors", IEEE Electron Device Lett., vol. 28, pp. 760-762, 2007.

[12] G. Liang, et al., "Ballistic graphene nanoribbon metal-oxide-semiconductor field-effect transistors: A full real-space quantum transport simulation", J. Appl. Phys., vol. 102, 054307, 2007.

[13] P. Zhao and J. Guo, "Modeling edge effects in graphene nanoribbon field-effect transistors with real and mode-space methods", J. Appl. Phys., vol. 105, 034503, 2009.

[14] R. Grassi et al., "Tight-binding and effective mass modeling of armchair graphene nanoribbon FETs", Solid State Elec., vol. 53, pp. 462-467, 2007.

[15] V. Nam Do, V. Hung Nguyen, P. Dollfus, and A. Bournel, "Electronic transport and spin-polarized effects of relativistic-like particles in graphene structures", J. Appl. Phys., vol. 104, 063708, 2008.

[16] V. Hung Nguyen, A. Bournel, V. Lien Nguyen, P. Dollfus, "Resonant tunneling and negative transconductance in single barrier bilayer graphene structures", Appl. Phys. Lett., vol. 95, 232115, 2009.

[17] Y.M. Tan et al., "Measurement of scattering Rate and minimum conductivity in graphene", Phys. Rev. Lett. Vol. 99, 246803, 2007.

[18] A. Cresti et al., "Charge Transport in Disordered Graphene-Based Low Dimensional Materials", Nano. Res., vol. 1, pp. 361-394, 2008.

[19] V. Nam Do and P. Dollfus, "Modelling of metal-graphene coupling and its influence on transport properties in graphene at the charge neutrality point", J. Phys. Condens. Matter, 2010, in press.

[20] R. Golizadeh-Mojarad and S. Datta, "Effect of contact induced states on minimum conductivity in graphene", Phys. Rev. B, vol. 79, 085410, 2009.

[21] F. Xia, D. B. Farmer, Y.-M. Lin, and P. Avouris, "Graphene field-effect transistors with high On/Off current ratio and large transport band gap at room temperature, Nano Lett., vol. 10, pp. 715-718, 2010.

[22] N. Tombros et al., "Electronic spin transport and spin precession in single graphene layers at room temperature", Nature, vol. 448, pp. 571-575, 2007.

[23] H. Haugen, D. Huertas-Hernando, and A. Brataas, "Spin transport in proximity-induced ferromagnetic graphene", Phys. Rev. B, vol. 77, 115406, 2008.

[24] V. Hung Nguyen, A. Bournel, C. Chassat, P. Dollfus, "Quantum transport of Dirac fermions in graphene field effect transistors", Proc. SISPAD 2010, pp. 9-12, 2010.

[25] L. Liao et al., "Sub-100 nm Channel Length Graphene Transistors", Nano Lett., 2010; DOI: 10.1021/nl101724k.